

Trapping of carriers in single quantum wells with different configurations of the confinement layers

H.-J. Polland,* K. Leo, K. Rother, and K. Ploog

*Max-Planck-Institut für Festkörperforschung, Heisenbergstrasse 1,
D-7000 Stuttgart 80, Federal Republic of Germany*

J. Feldmann, G. Peter, and E. O. Göbel

Fachbereich Physik, Philipps-Universität Marburg, Renthof 5, D-3550 Marburg, Federal Republic of Germany

K. Fujiwara, T. Nakayama, and Y. Ohta

*Central Research Laboratory, Mitsubishi Electric Corporation, Amagasaki 661, Japan
(Received 15 March 1988)*

This paper reports detailed experimental studies of low-temperature carrier trapping in GaAs/Al_xGa_{1-x}As single quantum wells with 5 nm and 1.2 nm thickness, respectively, with different confinement structures. Trapping efficiency and trapping dynamics are studied by means of photoluminescence, photoluminescence excitation spectroscopy, and picosecond luminescence spectroscopy. We obtain trapping efficiencies of about 40% for both the single quantum wells without additional confinement and separate-confinement-heterostructure quantum wells. The percentage of trapped carriers increases to about 60% to 80% for quantum wells cladded by graded-index separate-confinement heterostructures with parabolic band-gap profile. The maximum trapping efficiency of about 100% has been observed for a separate-confinement heterostructure with a linear band-gap profile. Interlayer well width fluctuations are found to be unimportant for the trapping behavior in our samples. Trapping times are appreciably shorter than the rise times of the quantum well photoluminescence, which are between 60 and 100 ps for the different structures. Surface recombination in the 0.2- μ m-thick Al_xGa_{1-x}As cladding layer does not reduce the trapping efficiency of the single quantum well without additional confinement compared with the separate-confinement heterostructure. An effective trapping area with about 80 nm width can be deduced on the basis of these results for the quantum-well structures with ungraded cladding layers.

I. INTRODUCTION

The investigation of the carrier trapping mechanism in quantum wells (QW's) is of particular interest from a fundamental physics as well as device orientated point of view. Theoretically, the problem can be separated into two parts, namely, (i) a classical transport problem described by the continuity equation including recombination, diffusion, and, in the presence of electric fields, drift of the carriers in the barrier material of the QW, and (ii) a quantum-mechanical problem describing the capture of a carrier into the QW taking into account the phonon coupling strength, wave functions of the initial and final states, energy levels, and phonon dispersion. So far, different conclusions for the trapping efficiency and trapping times have been drawn. A pronounced decrease of the carrier collection from the cladding layers into the QW's has been predicted for well thicknesses L_z smaller than the LO-phonon-scattering-limited carrier mean free path.¹⁻³ Instead, quantum-mechanical calculations have revealed a significant influence of resonant states in the confinement layers on carrier capture times for separate-confinement heterostructures⁴⁻⁷ and structures with graded barriers.⁸ Furthermore, resonance effects in the carrier-LO-phonon interaction have been predicted for specific QW thicknesses due to the quasi-two-dimensional properties of the phonon modes.⁹⁻¹¹ Experimentally, the

trapping behavior has been studied for GaAs/Al_xGa_{1-x}As QW's by means of time-resolved cathodoluminescence,¹² time-resolved photoluminescence,¹³ photoluminescence excitation spectroscopy,¹⁴ and excitation intensity dependent photoluminescence.¹⁵

The trapping behavior also essentially determines the properties of optoelectronic quantum well devices, in particular semiconductor lasers. The performance of semiconductor lasers is generally improved in separate-confinement-heterostructure lasers compared to conventional lasers since optical confinement and carrier confinement can be optimized separately by the proper design of the active layer and separate confinement layer.^{16,17} An additional improvement in laser performance, e.g., decrease of threshold current, is expected and commonly observed for QW lasers, where the active layer thickness becomes small and comparable with the de Broglie wavelengths of the confined, two-dimensional electrons and holes.¹⁸⁻²³ These advantageous features are attributed to the steplike electronic density of states in the quantum well layers leading to a significant enhancement of available excited states close to the bottom of the bands.^{21,22} Unfortunately, the salient features of separate-confinement-heterostructure quantum-well lasers are only observed for active layers with a thickness ≥ 8 nm.^{1,20,23} With graded-index waveguide separate-confinement lasers (GRIN-SCH), as introduced by

Tsang,^{24,25} however, low threshold currents can be achieved also for well thicknesses below 8 nm. The structure includes cladding layers, where the band gap is no longer constant but varies between a small value at the position close to the well to larger values for larger distances. Since then, GRINSCH structures have been successfully grown by molecular-beam epitaxy,^{24–35} and metalorganic chemical-vapor deposition.^{20,23,36–46} The novel structures allow to decrease the threshold current by more than a factor of 2 as compared to separate-confinement-heterostructure lasers.^{20,23} In addition, the coefficient T_0 which characterizes the temperature dependence of the threshold current can be as high as 190°C in GRINSCH structures, whereas for the regular separate-confinement heterostructures a coefficient T_0 below 150°C has been always measured.^{23,24} All these advantageous features are supplemented by the fact that in the GRINSCH structures the small overlap of the thin gain region with the optical field provides good higher-order transversal mode discrimination and thus almost ideal Gaussian intensity profiles²⁴ and low transparency currents.⁴⁷

Several plausible reasons have so far been proposed and demonstrated in order to explain the good optical properties and the low threshold current of GRINSCH structures as compared with separate-confinement heterostructures. (i) Good optical confinement⁴⁸ and an optimized overlap of gain and light distribution can be tailored.²³ (ii) Low internal losses by free-carrier absorption due to the small confinement factor.⁴⁷ (iii) An enhancement of carrier collection due to the intrinsic electric field in the graded region (funneling) which is most important for GRINSCH structures with active layer thicknesses below 10 nm.^{21,23,42} Experimental evidence for increased carrier collection in GRINSCH structures with a 5-nm single quantum well has been given recently.⁴⁹ (iv) Carrier population in the confining layer can become significant at threshold in particular of thin QW's with high confinement energy. It therefore has been suggested that competing recombination of carriers in the confinement layers is weaker in GRINSCH structures than in separate-confinement heterostructures due to the lower density of states.³⁹

In this paper we consider the influence of the configuration of the confinement layers for quantum-well layer thicknesses (L_z) of 5 nm and 1.2 nm on carrier trapping dynamics and efficiencies in GaAs/ $\text{Al}_x\text{Ga}_{1-x}\text{As}$ quantum-well structures. The paper extends data of a recently published letter,⁴⁹ where trapping efficiencies and trapping times have been reported for a 5-nm unconfined single quantum well (SQW), a separate-confinement-heterostructure (SCH) quantum well, and linearly graded and parabolically graded GRINSCH structures. In particular, data for a very thin QW ($L_z = 1.2$ nm) also are included. The outline of this paper is as follows: Following this introduction, Sec. II describes our experimental techniques and the sample configurations. In Sec. III the results of photoluminescence and photoluminescence excitation spectroscopy with excitation energies up to 2 eV will be presented in order to characterize the optical properties of the samples. In Sec. IV we compare photo-

luminescence and photoluminescence excitation spectra for different excitation and detection energies, respectively. These data elucidate that selective carrier trapping at distinguished lateral positions is not important for our samples. Section V describes the evaluation of the trapping efficiencies from excitation spectroscopy experiments and the different confinement structures for the QW with $L_z = 5$ nm are compared. In addition, picosecond photoluminescence experiments are performed to investigate the kinetics of the trapping process. Section VI is dedicated to a comparative study of the photoluminescence properties of a separate-confinement heterostructure and an unconfined single quantum well and reveals important information about the influence of surface recombination on the carrier trapping dynamics and efficiency. The intensity dependence of carrier trapping is described in Sec. VII. Photoluminescence, photoluminescence excitation, as well as time-resolved photoluminescence spectroscopy are also performed on 1.2-nm-thick single quantum wells which are either unconfined or confined by a parabolically graded structure as will be described and discussed in Sec. VIII. We finally will give a short summary which concludes this work.

II. EXPERIMENT

We have studied the trapping of carriers from $\text{Al}_x\text{Ga}_{1-x}\text{As}$ cladding layers into the QW in six different structures. The samples are grown by molecular-beam epitaxy⁵⁰ (MBE) on a semi-insulating GaAs substrate. We use two nominal well widths of $L_z = 5$ nm and $L_z = 1.2$ nm for the GaAs single quantum wells which are confined by four different structures. Figure 1 shows cross sections of the structures: (a) The unconfined single quantum well (SQW) consists of the quantum well cladded by $\text{Al}_{0.3}\text{Ga}_{0.7}\text{As}$ layers. (b) The separate-confinement heterostructure (SCH) comprises additional outer layers of $\text{Al}_{0.6}\text{Ga}_{0.4}\text{As}$. (c) In the linearly graded heterostructure (L-GRINSCH) the alloy concentration x of the cladding layer is linearly varied between $x = 0.3$ and $x = 0.6$. (d) The parabolically graded heterostructure (P-GRINSCH) exhibits a parabolic variation of the band gap of the cladding layer between $x = 0.3$ and $x = 0.6$. The thickness of the $x = 0.3$ or graded cladding layers is $0.2 \mu\text{m}$ on either side of the quantum well. For the 5-nm-thick quantum wells all four structures have been investigated whereas for the 1.2-nm-thick samples we have only examined the carrier trapping in the structures (a) and (d).

During the experiments the samples are kept at 6 K. The quantum wells are photoexcited by picosecond pulses generated by a synchronously mode-locked dye laser. The photon energy of the dye laser emission can be continuously varied between 1.5 and 2 eV. We use the laser dyes rhodamine-6G, rhodamine-101, DCM, pyridine-2, and styryle-9. The pulse duration depends on the used dye and varies between 3 and 7 ps. The repetition rate is 80 MHz. The excitation density has been evaluated from the power of the exciting light and the laser spot size on the sample. Accurate values for the diameter of the spot size are obtained by scanning a calibrated pin hole ($5 \mu\text{m}$

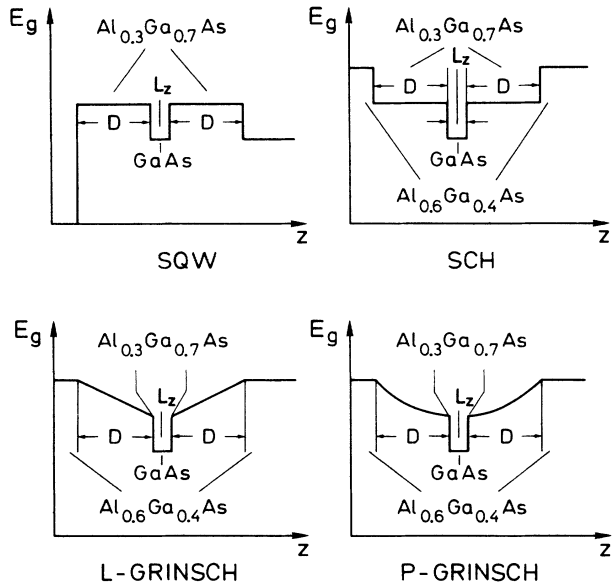


FIG. 1. Band-gap profiles of the different structures used in the experiments.

diameter) across the laser spot. The density of the excited carriers depends on the number of absorbed photons and is between $2.5 \times 10^9 \text{ cm}^{-2}$ and $1 \times 10^{12} \text{ cm}^{-2}$ for the direct and between $3 \times 10^9 \text{ cm}^{-2}$ and $8 \times 10^{12} \text{ cm}^{-2}$ for the indirect excitation. Time-integrated spectra are taken with a 0.8-m double monochromator and a GaAs photomultiplier. Time-resolved measurements are obtained with a synchroscan streak camera and a grating spectrometer. The spectral resolution amounts to 1.5 meV. The time resolution of 20 ps is limited by the temporal broadening by the spectrometer and the trigger jitter of the streak camera.

III. SAMPLE CHARACTERIZATION

Photoluminescence excitation spectra (PLE) and time-integrated photoluminescence (PL) spectra have already been published for 5-nm-thick SCH and P-GRINSCH samples.⁴⁹ Here we show in Fig. 2 the results for the SQW and the P-GRINSCH of the 1.2-nm-thick samples. The energies of the quantum well PL at 1.776 and 1.807 eV for the SQW and the P-GRINSCH, respectively, are close to the absorption edge of the $\text{Al}_{0.3}\text{Ga}_{0.7}\text{As}$ cladding layer at 1.846 and 1.890 eV due to the small well width and large confinement energies of electrons and holes. The Stokes shift between the PL peak position and the heavy hole peak in the excitation spectra is between 9 and 14 meV which is comparable to the half-width of the spectra of ≈ 10 meV. The splitting between heavy hole and light hole transition is determined from the PLE and amounts to 18 meV. A strong increase of the PL intensity for excitation energies ≥ 1.846 eV for the SQW [Fig. 2(a)] reflects the sharp increase of the number of photoexcited electron-hole pairs due to the onset of the absorption in the $\text{Al}_{0.3}\text{Ga}_{0.7}\text{As}$ cladding layer. Additional PL of the $\text{Al}_{0.3}\text{Ga}_{0.7}\text{As}$ at 1.841 eV is also observed in the SQW

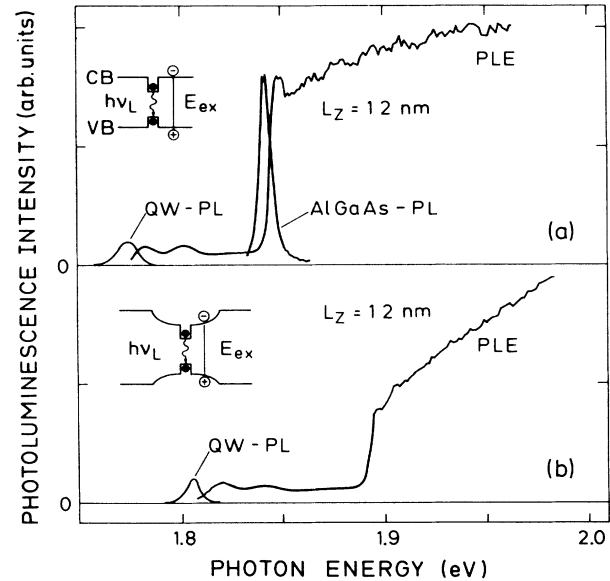


FIG. 2. Photoluminescence excitation spectra and time-integrated photoluminescence spectra of a SQW (a) and P-GRINSCH (b) with a nominal quantum-well thickness of $L_z = 1.2$ nm.

for excitation energies ≥ 1.845 eV. The fact that the $\text{Al}_{0.3}\text{Ga}_{0.7}\text{As}$ PL intensity is even higher than the quantum well PL intensity under resonant excitation of the $\text{Al}_x\text{Ga}_{1-x}\text{As}$ demonstrates that a significant number of carriers radiatively recombine in the cladding layers. Similar results have been already reported for the 5-nm-thick SCH.⁴⁹ The excitation spectrum of the P-GRINSCH structure in Fig. 2(b) is very similar to that of the 5-nm-thick sample.⁴⁹ The moderate increase of the PL intensity of the QW for energies ≥ 1.89 eV is due to the gradual increase of absorbance in the parabolically graded cladding layer. Radiative recombination in the confinement layers is absent since no PL around 1.890 eV can be observed, in accordance with the results for the 5-nm L-GRINSCH and P-GRINSCH.

Table I summarizes the optical parameters of the six different samples. The calculated well widths are obtained by solving the Schrödinger equation for quantum wells with finite barrier height. The Al content x of the confinement layer which determines the barrier height is evaluated from the onset of the absorption of the cladding layer (last column of Table I) assuming that the band-gap energy E_g^x of $\text{Al}_x\text{Ga}_{1-x}\text{As}$ is given by $E_g^x = 1.519 \text{ eV} + 1.247x$.⁵¹ L_z then is varied to obtain agreement between the calculated confinement energies for electrons and heavy holes and the sum of the energy of the hh transition and the exciton binding energy, assuming a binding energy of 10 meV for both 1.2-nm- and 5-nm-thick QW's (Ref. 52) and a distribution of the band-gap discontinuities between conduction and valence bands of 57%:43%. The model also considers the non-parabolicity of the conduction band.⁵³ Effective electron and heavy-hole masses are $(0.0665 + 0.0835x)m_0$ and $(0.34 + 0.42x)m_0$.⁵⁴ As can be seen from Table I the cal-

TABLE I. Optical parameters of the quantum-well samples used for the experiments.

Sample no.	Type	L_z (nm) nominal	L_z (nm) calculated	QW energy (eV)	PL FWHM (meV)	hh energy (eV)	lh energy (eV)	$\text{Al}_x\text{Ga}_{1-x}\text{As}$ PL energy (eV)	PL FWHM (meV)	$\text{Al}_x\text{Ga}_{1-x}\text{As}$ absorption edge (eV)
1	SQW	5.0	5.6	1.582	3.2	1.586	1.604	1.806	3.4	1.805
2	SCH	5.0	4.7	1.603	10.5	1.605	1.628	1.841	4.1	1.842
3	L-GRINSCH	5.0	4.5	1.608	17.5	1.625	1.642			1.850
4	P-GRINSCH	5.0	4.9	1.600	9.5	1.601	1.625			1.844
5	SQW	1.2	1.1	1.776	10.0	1.785	1.803	1.843	1.6	1.846
6	P-GRINSCH	1.2	1.1	1.807	8.0	1.821	1.841			1.890

culated well widths are close to the nominal values as determined from the MBE growth parameters. From the half-width of the QW PL it becomes obvious that inhomogeneous broadening can be different for the various samples. In particular, the half-width of the PL spectrum and the Stokes shift between the PL peak position and the hh transition in the excitation spectrum in samples 1 and 3 differ by more than a factor of 5. However, it will be shown below that the moderate optical quality of sample 3 does not reduce the carrier trapping efficiency. Table I also depicts the peak positions of the hh and lh transitions as obtained from PLE. Photoluminescence of the $\text{Al}_x\text{Ga}_{1-x}\text{As}$ confinement layers is only observed for the SQW and SCH. The Stokes shift between the PL peak position and the $\text{Al}_x\text{Ga}_{1-x}\text{As}$ absorption edge is between 1 and 3 meV and is always below the half-width of the $\text{Al}_x\text{Ga}_{1-x}\text{As}$ PL. The energies for the onset of the confinement layer absorption which has been deduced from the excitation spectra are listed in the last column of Table I. The differences of the energy of the absorption edge between 1.805 and 1.890 eV for the different samples corresponds to differences in the Al content in the confinement layers between $x=0.23$ and $x=0.35$.

The spectrally integrated photoluminescence intensity of the QW's has been measured for direct excitation, i.e., at photon energies where the cladding layer is transparent and carriers are photoexcited in the QW only. The measured values which are proportional to the quantum efficiency are normalized to that of the SQW with nominal thickness $L_z=1.2$ nm and are listed in Table II. Although the number of absorbed photons is approximately the same for all the samples [αL is about constant for

different thicknesses L_z (Ref. 55)], we observe differences in the luminescence efficiency. Under direct excitation with $h\nu_L=2.039$ eV photoluminescence is additionally observed from the $\text{Al}_{0.3}\text{Ga}_{0.7}\text{As}$ cladding layers in the case of the SQW and the SCH. For the P-GRINSCH and L-GRINSCH, no $\text{Al}_x\text{Ga}_{1-x}\text{As}$ photoluminescence can be observed, demonstrating that the photoexcited electrons and holes are rapidly separated or trapped.

For the interpretation of the results in the following sections it is important to know the dependence of the photoluminescence yield on the number of photoexcited electron-hole pairs. We have therefore varied the excitation intensity and measured the spectrally and time-integrated photoluminescence intensity for all samples. Figure 3 shows experimental results for the SQW with $L_z=5$ nm [Fig. 3(a)] and $L_z=1.2$ nm [Fig. 3(b)] as an example. The dependence of the PL intensity on the photoexcited carrier density is linear up to densities of $1 \times 10^{12} \text{ cm}^{-2}$. A trend towards a weaker dependence is observed in the case of indirect excitation for higher carrier densities. It is obvious from Fig. 3 that the PL intensity is lower for indirect excitation as compared to direct excitation in the entire excitation density regime, which already reflects the incomplete carrier trapping in the case of indirect excitation of the SQW.

IV. HOMOGENEITY OF CARRIER TRAPPING

An influence of the well width on the trapping times and trapping efficiency has been predicted and experimentally found in some previous publications.^{14,15} Mishima *et al.*¹⁵ reported that the PL intensity depends non-

TABLE II. Relative photoluminescence intensities (spectrally and time integrated) of quantum-well and $\text{Al}_x\text{Ga}_{1-x}\text{As}$ recombination for the different samples.

Sample	L_z (nm)	Photoluminescence intensity	
		Direct excitation QW	Indirect excitation $\text{Al}_x\text{Ga}_{1-x}\text{As}/\text{QW}$
SQW	5.6	0.72	0.03
	1.1	1	0.01
SCH	4.7	0.36	0.15
	4.9	0.72	0
P-GRINSCH	1.1	0.83	0
	4.5	0.61	0

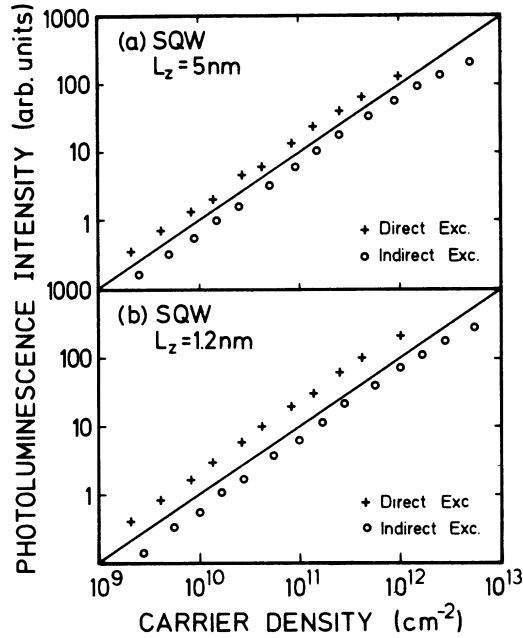


FIG. 3. Spectrally and time-integrated photoluminescence intensity of the QW recombination of the SQW with $L_z = 5$ nm (a) and $L_z = 1.2$ nm (b) vs two-dimensional carrier density for direct (+) and indirect excitation (O), respectively. In the case of indirect excitation the two-dimensional density is obtained by integrating the three-dimensional density over the length perpendicular to the QW, in which absorption occurred. The straight line is a guide for the eye representing a linear dependence.

linearly on the excitation intensity in samples containing several quantum wells with different widths and small barrier layers. A theoretical explanation of these results has been given by Murayama.⁷ Titkov *et al.*¹⁴ have measured excitation spectra in the vicinity of the $\text{Al}_x\text{Ga}_{1-x}\text{As}$ band-gap energy for a sample containing three single QW's with a thickness of 6.5, 13.5, and 27.7 nm, separated by barrier layers with a thickness of 23.3 nm. They have found a strong change in the shape of the excitation spectrum as a function of the detection wavelength within the spectral width of the emission of one particular QW which they have attributed to inhomogeneities in the carrier capture efficiency. Small intralayer well-width fluctuations lead to inhomogeneous broadening of the QW photoluminescence which may be accidentally accompanied by strong shifts of the resonant states in the barrier layer^{4,5} or the optical-phonon coupling.⁹⁻¹¹ The shifts of resonant states have been claimed to be responsible for the detection-wavelength-dependent changes in the excitation spectra.¹⁴

In order to examine whether well-width fluctuation in our samples can lead to inhomogeneities in the carrier trapping, we measure photoluminescence spectra in dependence on the excitation photon energy and photoluminescence excitation spectra as a function of the detection wavelength. Figure 4 shows PL spectra for the P-GRINSCH samples with $L_z = 5$ and 1.2 nm. Indirect

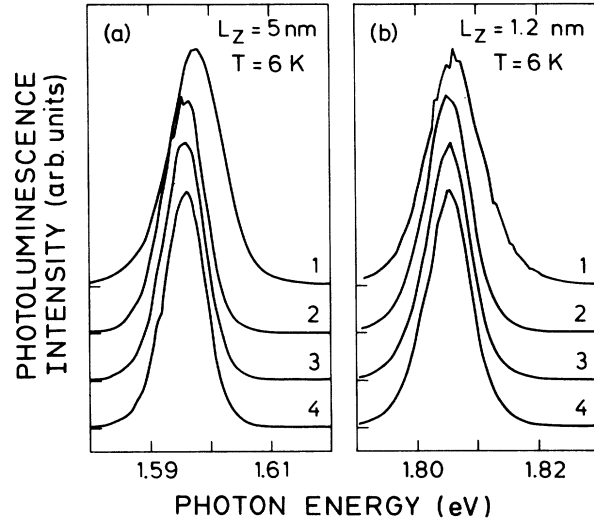


FIG. 4. Photoluminescence spectra of the QW emission for the P-GRINSCH with $L_z = 5$ nm (a) and 1.2 nm (b) for different excitation conditions as described in the text.

excitation with an intensity corresponding to a carrier density of 10^{11} cm^{-2} and an excitation energy which exceeds the onset of the absorption edge of the cladding layer by ≈ 80 meV and results in a relatively broad PL spectrum (curve 1) with the peak positions at 1.598 and 1.807 eV and a width [full width at half maximum (FWHM)] of 10 and 10.5 meV for the 5-nm- and 1.2-nm-thick QW's, respectively. A smaller width of the PL spectra and a slight shift of the PL peak position to lower energies is found for the same excitation intensity but an excitation energy chosen 15 meV below the onset of the absorption edge of the cladding layer. However, the number of photoexcited carriers is now strongly reduced to about $5 \times 10^9 \text{ cm}^{-2}$. In order to distinguish whether the mechanism of carrier trapping influences the shape of the PL spectrum or whether the spectral changes between spectrum 1 and 2 are due to differences in the carrier density, we have measured PL spectra for different excitation energies below and above the absorption edge of the cladding layer band-gap energy. For the excitation above the $\text{Al}_x\text{Ga}_{1-x}\text{As}$ band gap we have attenuated the excitation intensity in order to obtain the same spectrally integrated photoluminescence intensity of the QW, i.e., the same number of electron-hole pairs in the well. Curves 2, 3, and 4 in Fig. 4 represent spectra for excitation energies 15 meV below, in resonance, and 15 meV above the onset of the absorption edge of the cladding layer, respectively. The figure clearly shows the exact correspondence of the three different PL spectra indicating that the PL spectra depend only on the number of photoexcited electron-hole pairs. We can conclude that for all samples used in this work inhomogeneous broadening due to well-width fluctuations does not play an important role in the mechanism of carrier trapping.

Similar conclusions are obtained from the measurements of the photoluminescence excitation spectra. Figure 5 shows spectra for the 1.2-nm-thick SQW and the 5-

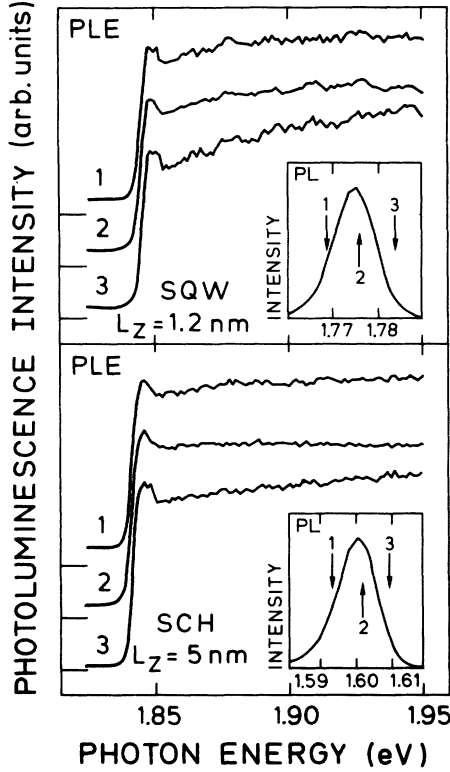


FIG. 5. Photoluminescence excitation spectra for the SQW with $L_z = 1.2$ nm and the SCH with $L_z = 5$ nm detected at different spectral positions (indicated by arrows) within the emission band of the QW.

nm-thick SCH. The curves have been measured for detection wavelengths on the low-energy side, on the high-energy side, and at the peak position as indicated by the arrows in the luminescence spectrum shown in the insets. The steep onset of the absorption at the band edge of the cladding layer at ≈ 1.84 eV is independent of the detection wavelength. In contrast to previously reported results,¹⁴ we do not find indications of inhomogeneities of the quantum-well photoluminescence with respect to the carrier trapping.

V. THE INFLUENCE OF THE CONFINEMENT STRUCTURE ON THE CARRIER TRAPPING

In the first part of this section we describe spectra for the four different confinement structures for the QW's with a nominal thickness of 5 nm. The comparison with calculated curves allows the quantitative evaluation of the carrier trapping efficiencies. The second part concerns with time-resolved photoluminescence measurements which allow determination of the influence of the configuration of the cladding layers on the carrier trapping times.

Figure 6 shows in the upper part photoluminescence excitation spectra for the SQW and the SCH (solid lines). The detection wavelengths are chosen at the peak position of the QW PL spectrum. The trapping efficiencies as

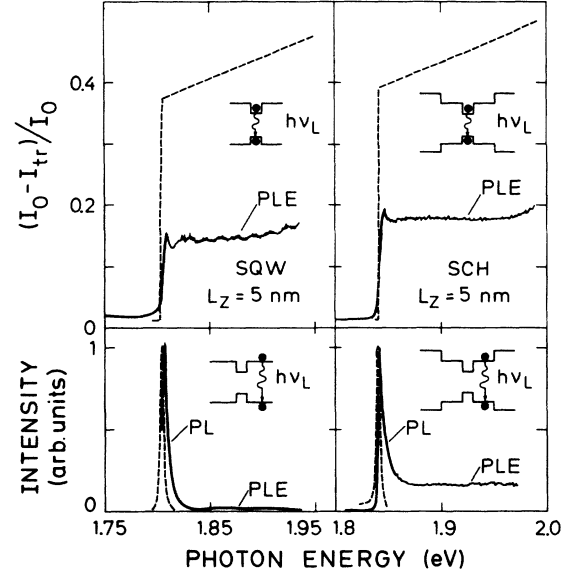


FIG. 6. Experimental photoluminescence excitation spectra of the quantum-well luminescence of the SQW and the SCH (solid lines) and calculated curves assuming a trapping efficiency of 100% (upper part) and photoluminescence and photoluminescence excitation spectra of the $\text{Al}_x\text{Ga}_{1-x}\text{As}$ cladding layers (lower part).

a function of the excitation photon energy $h\nu_L$ can be determined from the excitation spectra according to the following consideration. The QW-photoluminescence intensity as a function of excitation energy is described by

$$I_{\text{PL}}(h\nu_L) = C\eta(h\nu_L)\xi(h\nu_L)I_0, \quad (1)$$

where I_0 is the excitation intensity, $\eta(h\nu_L)$ is the percentage of absorbed photons, and $\xi(h\nu_L)$ denotes the trapping efficiency. The constant C includes the radiative efficiency of the QW, which is assumed to be independent on $h\nu_L$ since the quantum efficiency does not depend on carrier concentration (see Sec. III). The normalized intensity of the PLE spectra can therefore be expressed by the product of the trapping efficiency and the percentage of absorbed photons:

$$\frac{I_{\text{PL}}(h\nu_L)}{CI_0} = \eta(h\nu_L)\xi(h\nu_L). \quad (2)$$

The trapping efficiency $\xi(h\nu_L)$ is by definition equal to 1 for $h\nu_L$ below the band-gap energy of the $\text{Al}_x\text{Ga}_{1-x}\text{As}$. On the other hand, the values for $\eta(h\nu_L)$ for these energies are known either experimentally or can be estimated. For example, 1.1% of the exciting light is absorbed in 5-nm QW at a photon energy about 80 meV above the $n = 1$ transition.^{55,56} We are therefore able to calibrate the excitation spectra in terms of the percentage of absorbed photons. For photon energies above the $\text{Al}_x\text{Ga}_{1-x}\text{As}$ band gap, $\eta(h\nu_L)$ is given by

$$\eta(h\nu_L) = \frac{I_0 - I_{\text{tr}}(h\nu_L)}{I_0}, \quad (3)$$

where $I_{tr}(h\nu_L) = I_0 \exp[-\int \alpha(h\nu_L, z') dz']$ is the transmitted light intensity. The absorption coefficient $\alpha(h\nu_L, z)$ actually depends on z only in the GRINSCH structures. We have calculated $\eta(h\nu_L)$ for $h\nu_L$ larger than the $\text{Al}_x\text{Ga}_{1-x}\text{As}$ band gap on the basis of the absorption data reported in Ref. 57. The dashed lines in Figs. 6(a) and 6(b) show the corresponding curves. According to Eqs. (2) and (3) these calculated curves would coincide with the experimental PLE if the trapping efficiencies were equal to 1 as in the case of excitation with $h\nu_L$ smaller than the $\text{Al}_x\text{Ga}_{1-x}\text{As}$ band gap. The ratio of the calculated (dashed) and experimental (solid) curves thus yields directly the trapping efficiency $\xi(h\nu_L)$.

The comparison of the dashed and solid lines in Figs. 6(a) and 6(b) clearly shows that a significant amount of the photoexcited carriers in the confinement layers of the SQW and SCH is not trapped into the well. In addition, it can be seen that the presence of the outer barrier with $x = 0.6$ in the SCH does not significantly change the PLE spectrum indicating that the trapping efficiencies in the SQW and SCH are about equal. Figures 6(c) and 6(d) depict normalized photoluminescence spectra (dashed line) and PLE spectra for the $\text{Al}_{0.3}\text{Ga}_{0.7}\text{As}$ cladding layer. The photoluminescence intensity of the $\text{Al}_x\text{Ga}_{1-x}\text{As}$ layer under resonant excitation at 1.805 and 1.842 eV for the SQW and SCH, respectively, is comparable to the QW PL intensity. Obviously, a significant part of the carriers radiatively recombines in the cladding layer. A sharp decrease in the $\text{Al}_{0.3}\text{Ga}_{0.7}\text{As}$ PL intensity, however, is observed for higher excitation energies which levels at 1% and 15% of the maximum value for energies > 1.84 eV and > 1.81 eV for the SQW and SCH, respectively. The fact that no concomitant increase of the PL intensity in the QW is observed [Figs. 6(a) and 6(b)] indicates that nonradiative recombination in the $\text{Al}_{0.3}\text{Ga}_{0.7}\text{As}$ layer now has to be considered as well. (Note, however, that the PLE spectra of the $\text{Al}_x\text{Ga}_{1-x}\text{As}$ and the QW may have different absolute intensity scales, because the quantum efficiency for radiative recombination in the $\text{Al}_x\text{Ga}_{1-x}\text{As}$ is not known.) Nonradiative recombination is stronger in the SQW [Fig. 6(c)]. Obviously, surface recombination appreciably competes with radiative recombination in the SQW. A detailed discussion of the surface recombination will be given in the succeeding section.

Excitation spectra are also measured for the 5-nm P-GRINSCH and L-GRINSCH. In Fig. 7 the data (solid lines) are compared with the calculated percentage of absorbed photons (dashed lines). Obviously, the trapping efficiency is higher in the P-GRINSCH than in the SQW and SCH. The excitation spectrum comes close to the theoretical curve for the L-GRINSCH which corresponds to a trapping efficiency of about 100%.

The results of the carrier trapping efficiency for the four different confinement structures in dependence of the excess energy of the exciting light with energy $h\nu_L$ above the $\text{Al}_{0.3}\text{Ga}_{0.7}\text{As}$ band-gap energy are summarized in Fig. 8. The accuracy of these numbers is in the order of 10%. The number of photoexcited carriers which reach and recombine in the well amounts to about 40%

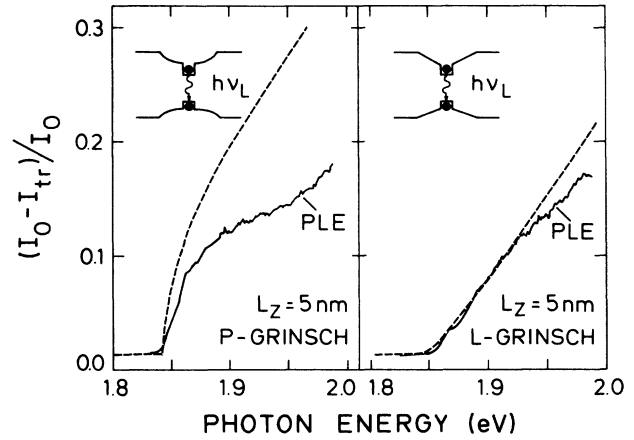


FIG. 7. Experimental photoluminescence excitation spectra for the 5-nm P-GRINSCH and L-GRINSCH (solid lines) and calculated curves for a trapping efficiency of 100%.

for the SQW and the SCH. Two competing channels to carrier trapping are responsible for this low trapping efficiency. (i) For resonant excitation of the $\text{Al}_x\text{Ga}_{1-x}\text{As}$ cladding layer strong radiative recombination in the $\text{Al}_x\text{Ga}_{1-x}\text{As}$ is observed [Figs. 6(c) and 6(d)]. (ii) The $\text{Al}_x\text{Ga}_{1-x}\text{As}$ photoluminescence decreases for higher excitation energies, whereas the photoluminescence of the QW remains essentially constant which demonstrates that nonradiative recombination in the cladding layer becomes dominant and competes with carrier trapping.

The trapping efficiencies are significantly larger in the P-GRINSCH and L-GRINSCH than in the SQW and SCH. The measured values for the L-GRINSCH are close to 100% in good agreement with the high internal

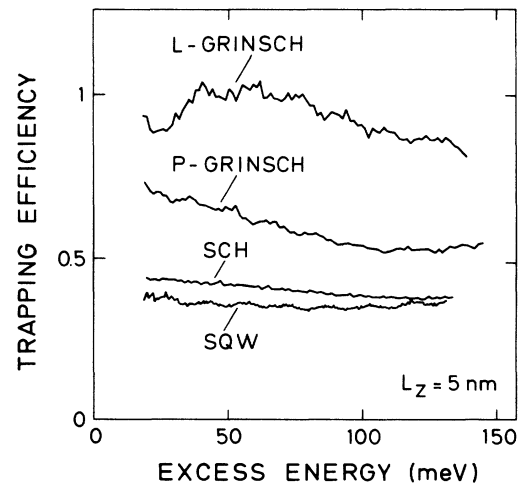


FIG. 8. Trapping efficiency vs excess photon energy of the exciting light with respect to the $\text{Al}_x\text{Ga}_{1-x}\text{As}$ band gap for the four different QW structures with $L_z = 5$ nm.

quantum efficiency of $90 \pm 10\%$ which has been found in L-GRINSCH lasers.^{41,42} However, in comparing our data and the laser data one has to realize that apart from the different temperatures at which these data are generally taken the initial spatial distribution of excited or injected carriers is different. In any case, the strong internal electric fields in the order of 10 kV/cm in the parabolically and linearly shaped confinement layer obviously lead to more efficient carrier trapping and thus suppress competing radiative and nonradiative recombination outside the well.

The suppression of competing channels in the GRINSCH structures can have different physical origins: (i) The distance from where carriers can reach the quantum well can be larger than in ungraded structures due to the drift of the carriers in the built-in electric field; (ii) carriers which become trapped in the $\text{Al}_x\text{Ga}_{1-x}\text{As}$ into shallow impurity or defect states can tunnel out of these states due to the electric field present in the GRINSCH; and (iii) radiative and nonradiative recombination of carriers within the $\text{Al}_x\text{Ga}_{1-x}\text{As}$ is reduced due to the partial spatial separation (polarization) of electrons and holes because of their different drift velocities. The difference between the L- and P-GRINSCH structures is possibly related to the different electric field distribution, which is constant throughout the barrier layers in case of the L-GRINSCH but approaches zero at the QW interface in case of the P-GRINSCH. However, we also have to consider that the initial optically excited carrier distribution is different in the L-GRINSCH and P-GRINSCH due to the different absorption profile. In addition, resonance effects may affect the trapping times, which also could influence the trapping efficiency.

We next report time-resolved photoluminescence experiments performed in order to investigate the kinetics of carrier trapping and recombination in the different structures. From the time behavior of the spectrally integrated QW photoluminescence we deduce the rise and decay times. The comparison of the rise times for the direct and indirect excitation with a photon energy below or above the absorption edge of the confinement layer allows conclusions regarding the trapping time. The intensity of the exciting light is adjusted in these experiments to values which provide the same time-integrated photoluminescence intensity of the QW for the direct and indirect excitation, i.e., the carrier densities in the QW are approximately equal.

Figure 9 depicts the temporal behavior of the QW photoluminescence (solid lines) for the indirect (i) and direct (d) excitation for the P-GRINSCH [Fig. 9(a)] and SCH [Fig. 9(b)]. The time behavior of the $\text{Al}_x\text{Ga}_{1-x}\text{As}$ luminescence is also included in the case of the SCH. Rise (τ_r) and decay (τ_d) times are obtained by fitting the data to the phenomenological expression

$$I(t) \propto [\exp(-t/\tau_r) - \exp(-t/\tau_d)], \quad (4)$$

which accounts for an exponentially decaying generation and recombination. An example for the fit is shown for the P-GRINSCH sample [dashed-dotted lines in Fig. 9(a)]. The accuracy of the numbers for τ_p and τ_d as ob-

tained by this procedure is about 20 ps. The results of the time-resolved luminescence can be summarized as follows. (i) The rise times of the QW photoluminescence for our samples differ already under direct excitation and are between 60 ps for the SCH and 100 ps for the SQW. These times slightly depend on the density of photexcited electron-hole pairs. We attribute the differences in the rise time to differences in the initial thermalization and relaxation processes, which are probably due to differences in the intralayer well-width fluctuations.^{58–61} (ii) The rise time of the photoluminescence of any samples remains almost unchanged under indirect excitation [note that the rise of the PL is also affected by the decay time; the rise times are always defined according to Eq. (4)]. (iii) Small differences in the decay times are observed for the direct and indirect excitation. We assume that charge separation due to the preferential trapping of one sort of carriers under indirect excitation, i.e., of electrons or holes, might weakly influence the radiative recombination in the QW. The mechanism for the differences in the decay times, however, is not completely understood so far. (iv) The decay time of the $\text{Al}_x\text{Ga}_{1-x}\text{As}$ photoluminescence for the SCH is much longer than the rise time of the QW photoluminescence, i.e., the recombination of the carriers in the $\text{Al}_x\text{Ga}_{1-x}\text{As}$ confinement layer is at least partly independent on the carrier trapping.

The experimental fact that the rise time of the photo-

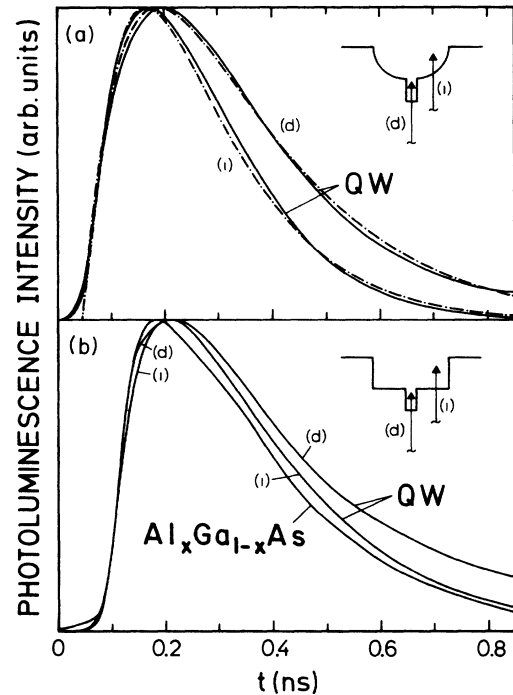


FIG. 9. Time behavior of the luminescence of the P-GRINSCH (upper part) and SCH (lower part) with $L_z = 5$ nm for direct (d) and indirect (i) excitation. The temporal variation of the $\text{Al}_x\text{Ga}_{1-x}\text{As}$ luminescence is also shown for the SCH QW. In the upper part the fit to the experimental results according to Eq. (4) is also shown, for example, by the dashed-dotted lines.

luminescence in all different samples is about the same for direct and indirect excitation, respectively, leads to the conclusion that the trapping times are appreciably shorter than the measured rise times. The rise time, on the other hand, for both direct and indirect excitation are determined by carrier relaxation and thermalization and exciton formation.⁶² As a consequence of this consideration, it seems likely that room-temperature measurements, where free carrier recombination dominates, would provide a better access to the trapping times. These experiments are presently under way. Anyway, the present results of the time-resolved luminescence do not show an apparent difference in the buildup of the QW luminescence if samples with and without a built-in electric field in the cladding layers are compared. We therefore conclude that the differences in trapping efficiency are basically due to differences in the effective volume available for carrier trapping and the differences in the initial spatial carrier distribution. This becomes evident by considering the results for the SQW and SCH which show about the same trapping efficiencies in spite of the different luminescence efficiency of the $\text{Al}_x\text{Ga}_{1-x}\text{As}$ luminescence.

VI. INFLUENCE OF SURFACE RECOMBINATION ON CARRIER TRAPPING

The photoluminescence efficiency of the $\text{Al}_x\text{Ga}_{1-x}\text{As}$ cladding layers under nonresonant excitations is appreciably lower (about a factor of 15) for the SQW as compared to the SCH. This difference is attributed to the existence of the free $\text{Al}_x\text{Ga}_{1-x}\text{As}$ surface in the SQW giving rise to strong nonradiative surface recombination,⁶³ as also revealed by the time behavior of the $\text{Al}_x\text{Ga}_{1-x}\text{As}$ luminescence. The time variation of the $\text{Al}_x\text{Ga}_{1-x}\text{As}$ luminescence of the 5-nm SQW and SCH under nonresonant, indirect excitation is depicted in Fig. 10. The PL decay is appreciably faster for the SQW demonstrating the effect of surface recombination. Note, however, that under nonresonant excitation the luminescence decay of the SCH is already strongly affected by nonradiative recombination as revealed by the excitation spectra of the $\text{Al}_x\text{Ga}_{1-x}\text{As}$ luminescence shown in Fig. 6. The radiative recombination efficiency in $\text{Al}_x\text{Ga}_{1-x}\text{As}$ obviously is high only for resonant excitation at the absorption edge of the $\text{Al}_x\text{Ga}_{1-x}\text{As}$. This behavior is attributed to exciton localization but a detailed discussion is beyond the scope of this paper and will be presented in a separate publication.

For the present topic it is important to note that the trapping efficiency of the SCH and SQW is the same in spite of the surface recombination in the SQW. Consequently, we have to conclude that for the geometrical dimensions of our samples carriers created in the vicinity of either the surface in case of the SQW or the $x=0.6/x=0.3$ interface in case of the SCH do not get trapped into the QW in both cases. The area of the excited $\text{Al}_x\text{Ga}_{1-x}\text{As}$ available as a reservoir for trapping of carriers into the QW is thus only a fraction of the entire excited volume. A lower limit for the dimension of this area perpendicular to the QW layers can be obtained

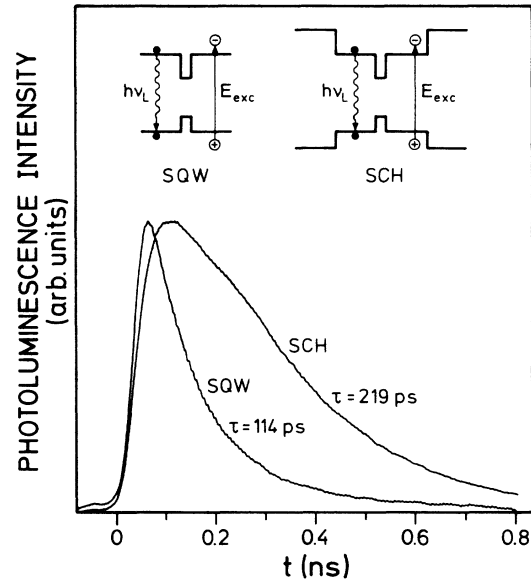


FIG. 10. Time-resolved photoluminescence of the $\text{Al}_x\text{Ga}_{1-x}\text{As}$ cladding layer of the 5-nm SQW and SCH.

from the measured trapping efficiency on the basis of the excitation profile ($\propto e^{-az}$) neglecting recombination in the $\text{Al}_x\text{Ga}_{1-x}\text{As}$ according to

$$\frac{e^{-(d-W_{tr})} - e^{-(d+W_{tr})}}{1 - e^{-2d}} = 0.4,$$

where $\alpha \approx 1.4 \times 10^4 \text{ cm}^{-1}$ is the absorption coefficient of the $\text{Al}_x\text{Ga}_{1-x}\text{As}$ slightly above the band-gap energy and $d = 0.2 \mu\text{m}$ is the width of the cladding layer. This very crude estimate yields a width of the effective trapping area of $W_{tr} \approx 80 \text{ nm}$. However, a more sophisticated analysis of the data is required to obtain more accurate numbers.

In summary we have shown in this section that in our samples with a cladding layer thickness of $0.2 \mu\text{m}$ the carrier trapping efficiency at low temperatures is not influenced by surface recombination in the $\text{Al}_x\text{Ga}_{1-x}\text{As}$. This result indicates that at low temperatures the width of the trapping area in ungraded cladding layers is restricted to about 100 nm for thin QW's ($L_z \approx 5 \text{ nm}$).

VII. CARRIER TRAPPING AT HIGH EXCITATION INTENSITIES ($n > 10^{12} \text{ cm}^{-2}$)

The results of Fig. 3 indicate a sublinear dependence of the luminescence intensity on the excited carrier density for $n > 10^{12} \text{ cm}^{-2}$, for indirect excitation, which may be interpreted by a decrease of the trapping efficiency. However, the values for the densities in Fig. 3 are deduced on the basis of a constant absorption coefficient independent on excitation power. In this section we will discuss the excitation spectra obtained at high excitation intensities.

Figure 11 depicts the QW (upper part) and

$\text{Al}_x\text{Ga}_{1-x}\text{As}$ photoluminescence excitation spectra for the SCH for four different carrier densities (at an excitation energy of 1.9 eV) of $5 \times 10^{10} \text{ cm}^{-2}$ (solid line), $2 \times 10^{11} \text{ cm}^{-2}$ (dashed line), $9 \times 10^{11} \text{ cm}^{-2}$ (dashed-dotted line), and $3 \times 10^{12} \text{ cm}^{-2}$ (dotted line). The spectrally integrated PL signal is divided by the excitation intensity in this plot. The luminescence intensity of the QW (upper part) decreases in the indirect excitation regime at high excitation densities, which might be due to a lower trapping efficiency. However, it is obvious that in particular in the near band-gap regime the shape of the excitation spectra in both the QW and $\text{Al}_x\text{Ga}_{1-x}\text{As}$ luminescence changes considerably. This change in the shape of the excitation spectra reflects the changes in absorption of the $\text{Al}_x\text{Ga}_{1-x}\text{As}$ with increasing carrier density which are in fact most pronounced near the band-gap edge where exciton resonances and Coulomb enhancement of the band-to-band transition strongly modify the absorption.⁶⁴ We therefore conclude that the decrease of the QW photoluminescence yield for energies $h\nu_L > 1.84 \text{ eV}$ at high excitation intensities is at least partly caused by the decrease of the percentage of absorbed photons, whereas the carrier trapping efficiency is not significantly changed. A quantitative evaluation of the trapping

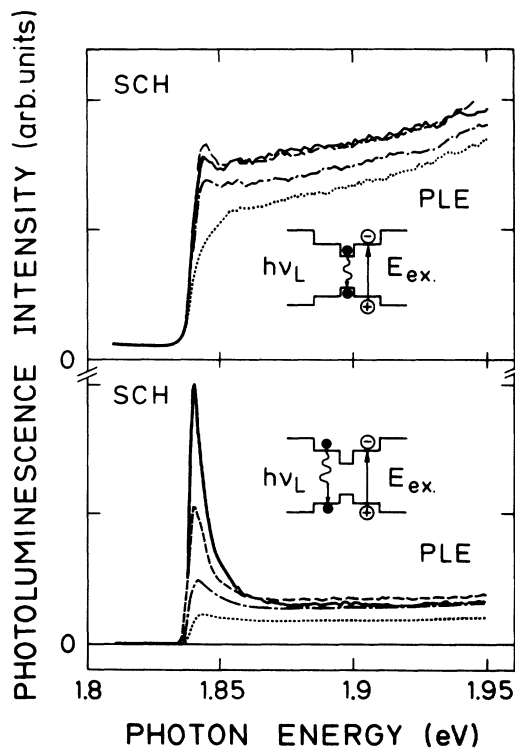


FIG. 11. Excitation spectra of the QW and $\text{Al}_x\text{Ga}_{1-x}\text{As}$ photoluminescence of the 5-nm SCH for different excitation densities. The carrier densities are estimated for a photon energy of 1.9 eV as described in the text (Sec. II) assuming a constant absorption coefficient and amount to $5 \times 10^{10} \text{ cm}^{-2}$ (solid line), $2 \times 10^{11} \text{ cm}^{-2}$ (dashed line), $9 \times 10^{11} \text{ cm}^{-2}$ (dashed-dotted line), and $3 \times 10^{12} \text{ cm}^{-2}$ (dotted line).

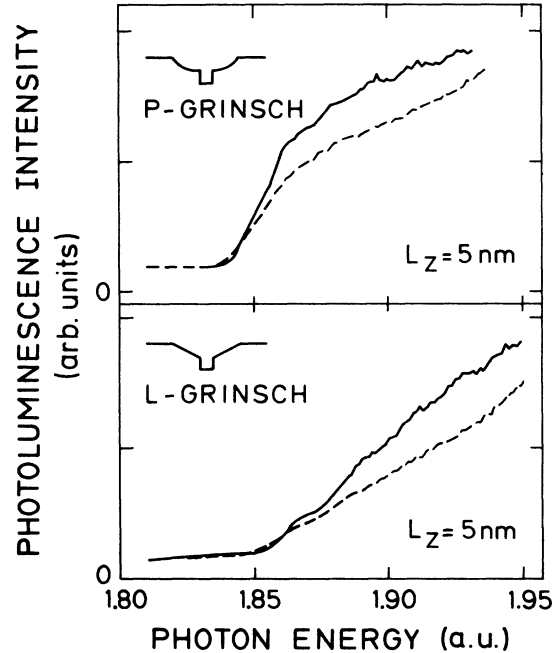


FIG. 12. Excitation spectra of the QW luminescence of the P-GRINSCH (upper) and L-GRINSCH (lower) for two excitation densities corresponding to carrier concentration of $5 \times 10^{10} \text{ cm}^{-2}$ (solid line) and $3 \times 10^{12} \text{ cm}^{-2}$ (dashed line). These values are determined from the excitation excitation density for a photon energy of 1.95 eV.

efficiency at high carrier densities is difficult since the absorption coefficient of $\text{Al}_x\text{Ga}_{1-x}\text{As}$ in this carrier density range has so far not been studied in great detail.

Similar results are observed for the P-GRINSCH and L-GRINSCH. Excitation spectra for the two samples are shown in Fig. 12 for two different carrier densities of $5 \times 10^{10} \text{ cm}^{-2}$ (solid lines) and $3 \times 10^{12} \text{ cm}^{-2}$ (dashed lines) (the densities are estimated at a photon energy of 1.95 eV). Again the photoluminescence yield decreases for higher excitation densities which can be partly attributed to the decrease of the absorption coefficient.

In conclusion of this section we believe that the decrease in the QW photoluminescence efficiency observed under indirect excitation with high intensities corresponding to carrier densities above 10^{12} cm^{-2} are basically caused by an intensity-dependent decrease of the absorption in the $\text{Al}_x\text{Ga}_{1-x}\text{As}$ and do not necessarily reflect a decrease of the trapping efficiency.

VIII. CARRIER TRAPPING IN 1.2-nm-THICK QUANTUM WELLS

In this section we report results on the influence of the well width on carrier trapping by comparing excitation spectra and time-resolved PL measurements for 1.2-nm- and 5-nm-thick SQW's and P-GRINSCH structures. Figure 13 shows photoluminescence excitation spectra for the 1.2-nm QW (solid lines).⁶⁵ The PLE spectra are quantitatively compared with the calculated curve for the

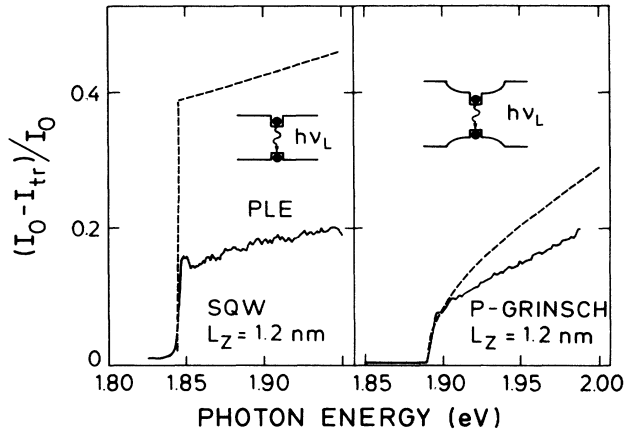


FIG. 13. Photoluminescence excitation spectra (solid lines) for the SQW and P-GRINSCH with $L_z = 1.2$ nm together with the calculated spectra (dashed lines) assuming a trapping efficiency of 100%.

percentage of absorbed carriers $\eta(h\nu_L)$ (dashed line). The curves for $\eta(h\nu_L)$ are obtained as described in Sec. V. However, the absorption coefficient for the $L_z = 1.2$ nm QW at energies below the band-gap energy of the $\text{Al}_x\text{Ga}_{1-x}\text{As}$ layer is extrapolated from data for thicker quantum wells^{55,56} since we are not aware of published data for the absorption coefficient for 1.2-nm-thick samples. For the evaluation we have assumed that the absorbance αL_z is independent on well thickness as in fact verified for QW with $L_z > 4$ nm.⁵⁵ We therefore have assumed the same value of 1.1% for the number of absorbed photons for direct excitation close to the $\text{Al}_x\text{Ga}_{1-x}\text{As}$ band edge for the QW with $L_z = 5$ nm and $L_z = 1.2$ nm. In fact, this assumption is valid in the model of the infinite quantum well in the single-particle picture.

Figure 14 shows the trapping efficiency in dependence on the excess energy above the $\text{Al}_x\text{Ga}_{1-x}\text{As}$ band gap. The dashed curves are obtained from the PLE spectra and the calculated curves (Fig. 13) and are compared with the trapping efficiency of 5-nm-thick wells (solid lines). Again we find that carrier trapping is more efficient in the P-GRINSCH than in the SQW. Trapping efficiencies of 0.4 are found for the 1.2-nm SQW whereas for the 1.2-nm P-GRINSCH ζ is between 0.73 (at 1.97 eV) and 0.86 (at 1.905 eV), which is slightly higher than for the 5-nm P-GRINSCH. However, we have to take into account that the values for the 1.2-nm QW have a larger uncertainty than for the 5-nm QW due to the assumption made in order to calibrate the excitation spectra. Nevertheless, the results indicate that the carrier trapping is similar in 1.2-nm- and 5-nm-thick wells.

Time-resolved measurements are also being performed for the 1.2-nm QW's. Again we use two different energies of the exciting light below and above the $\text{Al}_x\text{Ga}_{1-x}\text{As}$ band gap, respectively. Figure 15 shows the time behavior of the spectrally integrated photoluminescence of the SQW (upper part) and P-GRINSCH (lower part).

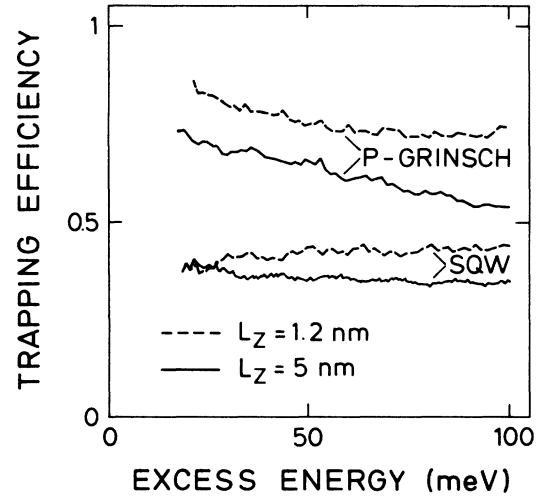


FIG. 14. Trapping efficiency as a function of excitation photon energy for the SQW and P-GRINSCH with $L_z = 1.2$ nm (dashed lines) in comparison with the values for $L_z = 5$ nm (solid lines).

time dependence of the $\text{Al}_x\text{Ga}_{1-x}\text{As}$ photoluminescence for indirect excitation is also included in the case of the SQW. No $\text{Al}_x\text{Ga}_{1-x}\text{As}$ luminescence of the P-GRINSCH is observed at low excitation intensities similar to the results of the 5-nm QW. The time behavior is roughly the same for direct and indirect excitation, simi-

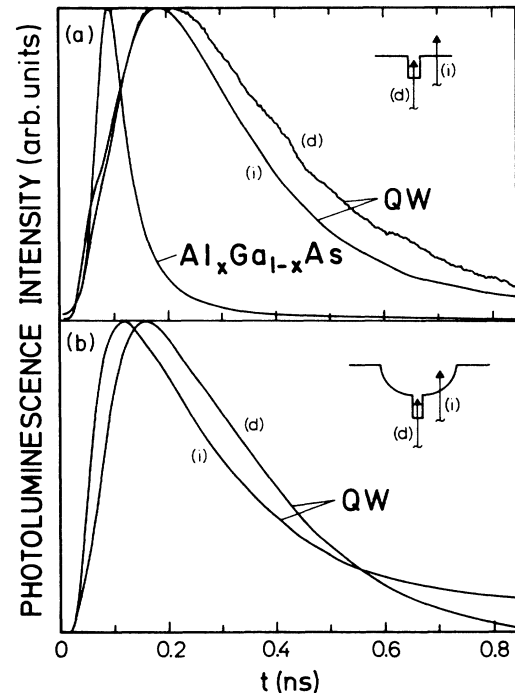


FIG. 15. Time-resolved QW photoluminescence of the SQW (upper part) and P-GRINSCH (lower part) with $L_z = 1.2$ nm for direct (d) and indirect (i) excitation. The time variation of the $\text{Al}_x\text{Ga}_{1-x}\text{As}$ luminescence is also depicted in case of the SQW.

lar to the results for the 5-nm QW. In particular, the rise time in the luminescence of the SQW is the same for direct and indirect excitation (the weak shoulder for direct excitation is due to incomplete suppression of the exciting laser, which is close to the spectral position of the QW luminescence because of the large confinement energy of the 1.2-nm QW). The rise time of the QW luminescence of the P-GRINSCH actually seems to be even faster for indirect excitation; however, it has to be realized that also the decay is slightly different for direct and indirect excitation, which actually explains the differences in the PL onset. Even though we do not understand this behavior in detail at present it is obvious that the indirect excitation does not introduce a delayed rise of the luminescence and thus the trapping times have to be appreciably smaller than the measured luminescence rise times similar to the results of the 5-nm QW.

The result that carrier trapping efficiencies as well as the photoluminescence decay times are similar in 1.2-nm- and 5-nm-thick wells is difficult to understand at a first glance because the confinement is expected to influence both the trapping¹⁻¹¹ and the recombination.⁶⁶ In order to estimate the degree of confinement in our samples we have calculated the envelope wave functions for electrons and holes. Figure 16 depicts the wave functions for the 1.2-nm and 5-nm SQW's. We have used the model of the finite QW as described in Sec. IV and the calculated energies and well width in Table I. The figure shows that the half-widths of the electron wave functions for the 1.1-nm and 5.6-nm QW (samples 1 and 5 in Table I) agree within 5% despite the strong differences in the well width by more than a factor of 5. This is of course due to the strong penetration of the wave function into the cladding layer for the 1.1-nm well. An evaluation of the confinement of the wave function can be obtained by calculating

$$\langle z^2 \rangle^{1/2} = \left(\frac{\int |\varphi(z)|^2 z^2 dz}{\int |\varphi(z)|^2 dz} \right)^{1/2}.$$

For electrons we obtain 1.95 nm in case of the 5.6-nm well, which is even smaller than the value of 2.51 nm for the 1.1-nm well.

The penetration of the wave functions into the cladding layer is smaller for holes than for electrons and here we obtain values for the spread of the heavy-hole wave functions of 0.97 and 1.39 nm for the 1.1-nm and 5.6-nm wells, respectively. In view of the fact that the electron-hole recombination and the carrier trapping are directly related to the spatial extent of the wave functions in z direction it is not surprising that the observed carrier lifetimes are similar in the 1.2-nm and 5-nm QW's. In addition, the fast carrier trapping time in the 1.2-nm QW and the similarity in the trapping efficiency of the 1.2-nm and 5-nm QW's are now qualitatively understood. However, conclusions cannot be drawn for the trapping times and efficiencies for QW's which have a well width between 1.2 and 5 nm. In this case the spread of the carrier wave functions could be significantly smaller leading to a reduction of the trapping efficiency and trapping probability. Further experiments have to be performed in order to elucidate this problem.

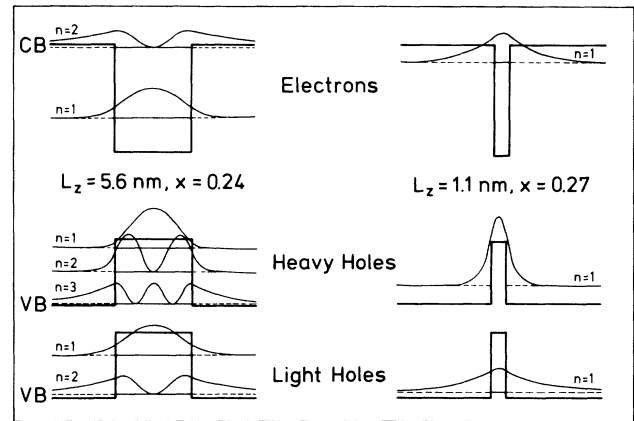


FIG. 16. Calculated spatial shape of the wave functions in the z direction (perpendicular to the QW layers for electrons as well as light and heavy holes for $L_z = 5.6$ and 1.1 nm, respectively).

IX. CONCLUSIONS

We have reported detailed studies on carrier trapping in GaAs single quantum wells, separate-confinement heterostructures, and GRINSCH structures. We have demonstrated that carrier trapping in linearly graded-index separate-confinement heterostructures is very efficient and can reach $\sim 100\%$. Quantum wells which are confined by other cladding profiles show a lower trapping efficiency due to the occurrence of competing channels: (i) radiative recombination in the $\text{Al}_x\text{Ga}_{1-x}\text{As}$ cladding layer for the single quantum well (SQW) and the quantum well with additional barrier layers (SCH), and (ii) nonradiative recombination in the cladding layer. The nonradiative recombination in the cladding layers is stronger in the SQW than in the SCH due to surface recombination, which, however, does not severely influence the carrier trapping efficiencies in the samples with $0.2\text{-}\mu\text{m}$ -thick cladding layers. The rise times of the QW photoluminescence are determined by relaxation and thermalization and no systematic difference are found for direct and indirect excitation. Consequently, the trapping times are appreciably shorter than the PL rise times, which are in the range of 60 to 100 ps for the different samples. We conclude from our data that the differences in trapping efficiency are basically caused by the different effective areas available for carrier trapping and by the different importance of the competing radiative and nonradiative recombination in the $\text{Al}_x\text{Ga}_{1-x}\text{As}$. In the ungraded structures carriers are effectively trapped by the quantum well only within a vicinity of the order of 100 nm. Outside of this area at least one sort of carrier remains trapped and recombines in the cladding layer or by surface recombination. For the GRINSCH structures with built-in electric fields on the order of 10 kV/cm the trapping area can be enlarged. We have shown that carrier trapping and recombination is similar in 1.2-nm and 5-nm-thick quantum wells, reflecting the fact that the electronic confinement is about the same. No significant changes in the trapping behavior are observed for carrier

densities up to 10^{12} cm^{-2} . At higher excitation intensities bleaching of the absorption is observed. Our investigations have demonstrated that the combination of photoluminescence, photoluminescence excitation spectroscopy, and picosecond time-resolved luminescence provides a useful tool to investigate the basic trapping processes in various quantum-well structures. Further insight will be gained by extending these experiments to higher temperatures and using even higher time resolution. In particular, the still open question on resonance effects in the carrier trapping may then be answered definitely.

Note added in proof. The trapping times in

InGaAs/InP QW's have been determined recently by subpicosecond photoluminescence experiments to be smaller than 1 ps [B. Deveaud, J. Shah, T. C. Damen, and W. T. Tsang, *Appl. Phys. Lett.* **52**, 1886 (1988)], consistent with our results.

ACKNOWLEDGMENTS

The expert technical assistance of M. Preis is gratefully acknowledged. Many thanks are expressed to J. Kuhl for fruitful discussions. The work at the University of Marburg is partly supported by the Deutsche Forschungsgemeinschaft.

*Present address: Fa. Dr. Johannes Heidenhain, D-8225 Traunreut, Federal Republic of Germany.

¹H. Schichijo, R. M. Kolbas, N. Holonyak, Jr., R. D. Dupuis, and P. D. Dapkus, *Solid State Commun.* **27**, 1029 (1978).

²R. D. Dupuis, P. D. Dapkus, R. M. Kolobas, N. Holonyak, Jr., and H. Schichijo, *Appl. Phys. Lett.* **33**, 596 (1978).

³J. Y. Tang, K. Hess, N. Holonyak, Jr., and P. D. Dapkus, *J. Appl. Phys.* **53**, 6043 (1982).

⁴J. A. Brum and G. Bastard, *Phys. Rev. B* **33**, 1420 (1986).

⁵J. A. Brum and G. Bastard, *Superlatt. Microstruct.* **3**, 51 (1987).

⁶S. V. Kozyrev and Y. Ya. Shik, *Fiz. Tekh. Poloprovodn.* **19**, 1667 (1985) [*Sov. Phys.—Semicond.* **19**, 1024 (1985)].

⁷Y. Murayama, *Phys. Rev. B* **34**, 2500 (1986).

⁸J. A. Brum, T. Weil, J. Nagle, and B. Vinter, *Phys. Rev. B* **34**, 2381 (1986).

⁹M. Babiker, M. P. Chamberlain, and B. K. Ridley, *Semicond. Sci. Technol.* **2**, 582 (1987).

¹⁰B. K. Ridley, in *Optical Properties of Narrow-Gap Low-Dimensional Structures*, edited by C. M. Sotomayor Torres, J. C. Portal, J. C. Mann, and R. A. Stradling (Plenum, New York, 1987), pp. 177.

¹¹M. Babiker and B. K. Ridley, *Superlatt. Microstruct.* **2**, 287 (1986).

¹²J. Christen, D. Bimberg, A. Steckenborn, and G. Weimann, *Appl. Phys. Lett.* **44**, 84 (1984).

¹³E. O. Göbel, H. Jung, J. Kuhl, and K. Ploog, *Phys. Rev. Lett.* **51**, 1588 (1983).

¹⁴A. Titkov, K. Kelting, K. Köhler, and A. Shik, in *Proceedings of the Eighteenth International Conference on the Physics of Semiconductors (ICPS), Stockholm, 1986*, edited by O. Engström (World Scientific, Göteborg, 1987), Vol. 1, p. 553.

¹⁵T. Mishima, J. Kasai, M. Morioka, Y. Sawada, Y. Murayama, Y. Katayama, and Y. Shiraki, *Surf. Sci.* **174**, 307 (1986).

¹⁶G. H. B. Thompson and P. A. Kirkby, *IEEE J. Quantum Electron.* **QE-9**, 311 (1973).

¹⁷W. T. Tsang, *Electron. Lett.* **16**, 939 (1980).

¹⁸C. Lindstrom, R. D. Burnham, D. R. Scifres, T. L. Paoli, and W. Streifer, *Electron. Lett.* **19**, 80 (1983).

¹⁹R. D. Burnham, W. Streifer, D. R. Scifres, C. Lindström, and T. L. Paoli, *Electron. Lett.* **18**, 1097 (1982).

²⁰S. D. Hersee, M. Krakowski, R. Blondeau, M. Baldy, B. de Crémoux, and J. P. Duchemin, *J. Cryst. Growth* **68**, 383 (1984).

²¹L. J. Ruyven, *J. Lumin.* **29**, 123 (1984).

²²N. Holonyak, Jr., R. M. Kolbas, R. D. Dupuis, and P. D. Dapkus, *IEEE J. Quantum Electron.* **QE-16**, 170 (1980).

²³S. D. Hersee, B. de Crémoux, and J. P. Duchemin, *Appl. Phys. Lett.* **44**, 476 (1984).

²⁴W. T. Tsang, *Appl. Phys. Lett.* **39**, 134 (1981).

²⁵W. T. Tsang, *Appl. Phys. Lett.* **40**, 217 (1982).

²⁶W. T. Tsang, R. A. Logan, and J. A. Ditzenberger, *Electron. Lett.* **18**, 845 (1982).

²⁷W. T. Tsang and R. L. Hartman, *Appl. Phys. Lett.* **42**, 551 (1983).

²⁸T. Fujii, S. Yamakoshi, K. Nanbu, O. Wada, and S. Hiyamizu, *J. Vac. Sci. Technol. B* **2**, 259 (1984).

²⁹O. Wada, S. Yamakoshi, T. Sanada, T. Fujii, T. Horimatsu, and T. Sakurai, *Electron. Lett.* **20**, 937 (1984).

³⁰O. Wada, T. Sanada, M. Kuno, and T. Fujii, *Electron. Lett.* **21**, 1025 (1985).

³¹T. Sanada, S. Yamakoshi, H. Hamaguchi, O. Wada, T. Fujii, T. Horimatsu, and T. Sakurai, *Appl. Phys. Lett.* **46**, 226 (1985).

³²H. Nobuhara, O. Wada, and T. Fujii, *Electron. Lett.* **21**, 718 (1985).

³³T. Fujii, S. Hiyamizu, S. Yamakoshi, and T. Ishikawa, *J. Vac. Sci. Technol. B* **3**, 776 (1985).

³⁴O. Wada, T. Sanada, N. Nobuhara, M. Kuno, M. Makiuchi, and T. Fujii, *Inst. Phys. Conf. Ser.* **79**, 685 (1985).

³⁵C. Harder, P. Buchmann, and H. Meier, *Electron. Lett.* **22**, 1081 (1986).

³⁶D. Kasemset, C. S. Hong, N. B. Patel, and P. D. Dapkus, *Appl. Phys. Lett.* **41**, 912 (1982).

³⁷R. D. Dupuis, R. L. Hartman, and F. R. Nash, *IEEE Electron Device Lett.* **EDL-4**, 286 (1983).

³⁸D. Feketa, K. T. Chan, J. M. Ballantyne, and L. F. Eastman, *Appl. Phys. Lett.* **49**, 1659 (1986).

³⁹J. Nagle, S. Hersee, M. Krakowski, T. Weil, and C. Weisbuch, *Appl. Phys. Lett.* **49**, 1325 (1986).

⁴⁰S. D. Hersee, M. Baldy, and P. Assenat, *J. Phys. (Paris) Colloq.* **43**, C5-19 (1982).

⁴¹S. D. Hersee, M. Baldy, P. Assenat, B. de Crémoux, and J. P. Duchemin, *Electron. Lett.* **18**, 870 (1982).

⁴²S. D. Hersee, B. Baldy, P. Assenat, B. de Crémoux, and J. P. Duchemin, *Electron. Lett.* **18**, 18 (1982).

⁴³M. Krakowski, P. Hirtz, R. Blondeau, S. D. Hersee, M. Baldy, B. de Crémoux, and J. P. Duchemin, *Electron. Lett.* **19**, 1082 (1983).

⁴⁴D. F. Welch, C. F. Schaus, and J. R. Shealy, *Appl. Phys. Lett.*

- 46, 121 (1985).
- ⁴⁵C. F. Schaus, J. R. Shealy, and L. F. Eastman, *J. Cryst. Growth* **73**, 37 (1985).
- ⁴⁶J. R. Shealy, *Appl. Phys. Lett.* **50**, 1634 (1987).
- ⁴⁷P. L. Derry, A. Yariv, K. Y. Lau, N. Bar-Chaim, K. Lee, J. Rosenberg, *Appl. Phys. Lett.* **50**, 1773 (1987).
- ⁴⁸R. F. Kazarinov and G. Tsarenkov, *Fiz. Tekh. Poloprovodn.* **70**, 297 (1976) [*Sov. Phys.—Semicond.* **10**, 178 (1976)].
- ⁴⁹J. Feldmann, G. Peter, E. O. Göbel, K. Leo, H.-J. Polland, K. Ploog, K. Fujiwara, and T. Nakayama, *Appl. Phys. Lett.* **51**, 226 (1987).
- ⁵⁰K. Mitsunaga, K. Kanamoto, M. Nunoshita, and T. Nakayama, *J. Vac. Sci. Technol. B* **3**, 627 (1985).
- ⁵¹H. C. Casey and M. B. Panish, *Heterostructure Lasers* (Academic, New York, 1978).
- ⁵²R. L. Greene, K. K. Bajaj, and D. E. Phelps, *Phys. Rev. B* **29**, 1807 (1984).
- ⁵³R. C. Miller, D. A. Kleinman, and A. C. Gossard, *Phys. Rev. B* **29**, 7085 (1984).
- ⁵⁴D. A. B. Miller, D. S. Chemla, T. C. Damen, A. C. Gossard, W. Wiegmann, T. H. Wood, and C. A. Burrus, *Phys. Rev. B* **32**, 1043 (1985).
- ⁵⁵Y. Masumoto, M. Matsuura, S. Tarucha, and H. Okamoto, *Phys. Rev. B* **32**, 4275 (1985).
- ⁵⁶H. Iwamura, H. Kobayashi, and H. Okamoto, *Jpn. J. Appl. Phys.* **23**, L795 (1984).
- ⁵⁷P. J. Pearah, W. T. Masselink, J. Klem, T. Henderson, H. Morkoç, C. W. Litton, and D. C. Reynolds, *Phys. Rev. B* **32**, 3857 (1985).
- ⁵⁸H. Stolz, D. Schwarze, W. von der Osten, and G. Weimann, in *Proceedings of the Eighteenth International Conference on the Physics of Semiconductors (ICPS), Stockholm, 1986*, edited by O. Engström (World Scientific, Göteborg, 1987), Vol. 1, p. 691.
- ⁵⁹J. Hegarty, M. D. Sturge, C. Weisbuch, A. C. Gossard, and W. Wiegmann, *Phys. Rev. Lett.* **49**, 930 (1982).
- ⁶⁰Y. Masumoto, S. Shionoya, and H. Kawaguchi, *Phys. Rev. B* **29**, 2324 (1984).
- ⁶¹T. Takagohara, *Phys. Rev. B* **31**, 6552 (1985).
- ⁶²R. Höger, E. O. Göbel, J. Kuhl, K. Ploog, and H.-J. Queisser, *J. Phys. C* **17**, L905 (1984).
- ⁶³R. J. Nelson and R. G. Sobus, *J. Appl. Phys.* **49**, 6103 (1978); R. J. Nelson, *J. Vac. Sci. Technol.* **15**, 1475 (1978).
- ⁶⁴H. Haug and S. Schmitt-Rink, *Prog. Quantum Electron.* **9**, 3 (1984).
- ⁶⁵A brief report of these data is given in H.-J. Polland, K. Leo, K. Ploog, J. Feldmann, G. Peter, E. O. Göbel, K. Fujiwara, and T. Nakayama, *Solid-State Electron.* **31**, 341 (1988).
- ⁶⁶J. Feldmann, G. Peter, E. O. Göbel, P. Dawson, K. Moore, C. Foxon, and R. J. Elliott, *Phys. Rev. Lett.* **59**, 2337 (1987).